Dalton Transactions

Hydrogen evolution, electron-transfer, hydride-transfer reactions in a nickel-iron hydrogenase model complex: A theoretical study of the distinctive reactivities for the conformational isomers of nickel-iron hydride

Journal:	*Dalton Transactions*
Manuscript ID	DT-ART-10-2021-003582.R1
Article Type:	Paper
Date Submitted by the Author:	06-Dec-2021
Complete List of Authors:	Isegawa, Miho; Kyushu University, I2CNER Matsumoto, Takahiro; Kyushu University, Department of Chemistry and Biochemistry Ogo, Seiji; Kyushu University, Chemistry and Biochemistry

ARTICLE

Hydrogen evolution, electron-transfer, hydride-transfer reactions in a nickel-iron hydrogenase model complex: A theoretical study of the distinctive reactivities for the conformational isomers of nickel-iron hydride

^Received 00th January 20xx,
Accepted 00th January 20xx

DOI: 10.1039/x0xx00000x

Miho Isegawa,*[a] Takahiro Matsumoto, [a] Seiji Ogo[a]

Hydrogen fuel is a promising alternative to fossil fuel. Therefore, efficient hydrogen production is crucial to elucidate the distinctive reactivities of metal hydride species, the intermediates formed during hydrogen activation/evolution in the presence of organometallic catalysts. This study uses density functional theory (DFT) to investigate the isomerizations and reactivities of three nickel-iron (NiFe) hydride isomers synthesized by mimicking the active center of NiFe hydrogenase. Hydride transfer within thse complexes, rather than a chemical reaction between the complexes, converts the three hydrides internally. Their reactivities, including their electron-stransfer, hydride-transfer, proton-transfer reactions, are investigated. The briding hydride complex exhibits a higher energy level for the highest occupied molecular orbital (HOMO) than the terminal hydride during the electron-trasnfer reaction. This energy level indicates that the bridging hydride is more easily oxidized and is more susceptible to electron transfer than the terminal hydride. Regarding the hydride-transfer reaction between NiFe hydride complex and methylene blue, the terminal hydrides exhibit larger hydricity and lower reaction barriers than the bridging hydride complexes. The results of energy decomposition analysis indicate that the structural deformation energy of the terminal hydride in the transition state is smaller than that of the bridging hydride complex, which lowers the reaction barrier of hydride transfer in the terminal hydride. To produce hydrogen, the rate-determining step is represented by the protonation of the hydride, and the terminal hydrides are thermodynamically and kinetically superior to the bridging ones. The differences in the reactivities of the hydride isomers ensure the precise control of hydrogen, and the theoretical calculations can be applied to design catalysts for hydrogen activation/production.

Introduction

Replacing fossil fuels with hydrogen ones will reduce the amount of carbon dioxide generated via fossil fuels; thus, developing catalysts that can efficiently activate/evolve hydrogen is crucial. Thus far, different organometallic complexes for activating/evolving H_2 have been synthesized.[1,2,3,4] Moreover, these catalytic functions and processes have been studied by various spectroscopic and X-ray analyses, and it has been shown that hydride complexes are produced as intermediates in the catalytic process. Hydride complexes are employed for hydrogen production and the conversion of nitrogen into ammonia, the reduction of CO_2, and the splitting of water.[5,6,7] Thus, it is essential to investigate the reactivities of hydride complexes for efficient hydrogen activation/evolution and a wide range of catalytic reactions.

A hydrogenase is an enzyme that reversibly catalyzes the activation of hydrogen. Organometallic complexes have been synthesized by mimicking the structure and function of the catalytic center of this enzyme. Hydrogenase can be classified into nickel-iron (NiFe), iron-iron (FeFe), and Fe hydrogenases. Regarding the binuclear hydrogenases (NiFe and FeFe), the coordination positions of their hydrides in the intermediate hydride complexes differ during the catalytic cycle. Bridging and terminal hydrides are generally detected in the catalytic cycles of NiFe and FeFe hydrogenases, respectively (Fig. S1).[8,9,10] The active centers of NiFe and FeFe hydrogenases comprise common ligands, such as CO and CN, and exhibit similar structural properties. Nevertheless, the coordination positions of the substrates in their intermediates are different, indicating the high sensitivities of the positions of the hydrides to metals and ligands and demonstrating the significance of the ligand design.

A recently synthesized model hydrogenase complex $[Ni^{II}(X)Fe^{II}(Cl)(CO)(L)]^+$ (X = *N,N'*-diethyl-3,7-diazanonane-1,9-dithiolato and L = 1,2-bis(diphenylphosphino)ethane)] (**1**, Fig. 1a) reversibly catalyzed heterolytic H_2 activation in an aqueous solution under ambient conditions (Fig. 1a).[11] The hydride complex, i.e., the intermediate of H_2 activation, underwent an isomerization reaction to produce three isomers (**2a**, **2b**, and **2c**; Fig. 1b). In Complex **2a**, the hydride ligand was located approximately halfway between Ni and Fe (μ-hydride). The hydride ligands in Complexes **2b** and **2c** were bound only to Fe (the terminal hydride). Further, the hydrides in Complexes **2b** and **2c** were in the trans- and cis-positions of the CO ligand, respectively. Furthermore, the isomers of these hydride complexes exhibited different reactivities to electron transfer (Fig. 1c), hydride-transfer (Fig. 1d), and proton-transfer reactions (Fig. 1e).

We elucidated the H_2 activation mechanism by the NiFe complex (1, Fig. 1a) in our previous theoretical study.[12] The NiFe complex activates hydrogen using frustrated Lewis pairs, forming hydride

[a] *International Institute for Carbon-Neutral Energy Research (WPI-I2CNER), Kyushu University, 744 Moto-oka, Nishi-ku, Fukuoka, 819-0395, Japan*

Electronic Supplementary Information (ESI) available: [details of any supplementary information available should be included here]. See DOI: 10.1039/x0xx00000x

complexes as intermediates. In this activation process, Fe acts as Lewis acids, and the added buffers act as Lewis bases. We have also previously investigated another NiFe complex[13] that activates/evolutes hydrogen in acetonitrile and elucidated the mechanisms of electron transfer, hydride transfer, and hydrogen evolution, from the bridging hydride complex.[14] However, those previous theoretical studies do not focus on the different reactivity of the hydride isomers. The coexistence of isomers with different reactivity may lead to the development of multifunctional catalysts, and it is important to understand the underlying factors that produce the differences in reactivity. While crystallization of thermodynamically unstable metal hydride complexes is generally difficult experimentally, DFT calculations allow structural optimization of the most stable structures as well as isomers in higher energy states with the same effort, which is useful for reactivity analysis.

So far, the changes in the reactivities of NiFe hydrogenase model complexes due to ligand alternation have been investigated by other groups. Makośetal et al.[15] investigated the effects of the ligand in the active site (Fe) on the interactions between Fe and H and Fe and H_2 to produce the NiFe hydrogenase mimicking complex;[13] they confirmed that the nature of the ligand correlated with these interactions. Brazzolotto et al.[16] demonstrated that the degree of CO inhibition in the NiFe hydrogenase model complex was changed during H_2 production via converting the Fe-coordinated cyclopentadienyl group into the pentamethylcyclopentadienyl group. However, the differences between the reactivities of the different isomers have not been studied.

Here, we first assigned infrared (IR) spectral peaks to the three isomers of the NiFe hydride complex to characterize their differences. Next, we clarified whether the isomerization of the hydride complexes proceeded via an intracomplex hydrogen transfer or an intercomplex chemical reaction. Additionally, the differences between the reactivities of the NiFe hydride complex in the three reactions were clarified via calculations. Specifically, we calculated the reaction energy and ionization potential (IP) of electron transfer during the electron-transfer reaction and investigated the oxidation tendency. Further, the hydricity and the reaction barrier were calculated to determine the one that controlled the reaction regarding the hydride-transfer reaction. Further, the reaction barrier of hydride transfer was divided into the contributions of the electrostatic interaction and structural deformation energy, revealing their crucial contributions. Finally, among the three hydrides, the isomers that accounted for the most efficient production of hydrogen were subjected to thermodynamic and kinetics investigations.

Computational details

The Gaussian 09 program performed all the computations in this study.[17] All the structures were fully optimized with no constraints by the BP86 functional[18,19] employing Grimme's empirical dispersion corrections (D3).[20] The BP86 functional has been employed to study the cluster model[21,22] and model complexes[23,24,14,25] of NiFe hydrogenase. Our previous study revealed that the calculated magneticity of the NiFe complex via this function correlated with the experimental result.[11] The Stuttgart/Dresden (SDD)[26] basis set and the associated effective core potential were employed for Ni and Fe, and the def2-SVP basis sets[27] (BSI) were employed for the other atoms. The solvation model based on density (SMD) implicit solvation model[28] was employed to determine the solvation effects of water (ε = 78.4), acetonitrile (ε = 35.688), and acetone (ε = 20.493). The vibrational frequencies were calculated at the same level of theory to confirm the minima and transition states (TSs) and to obtain the zero-point vibrational energy (ZPE) corrections and entropy contribution.

The thermal corrections were 298.15 K and 1 atm. The stationary points' connectivity was confirmed via th "pseudo" intrinsic reaction coordinate (IRC) approach[29]. The IRC calculations were performed for 20 steps from TS (in the forward and backward directions), and the resulting structures were fully functional optimized to obtain the minima. The potential energies were calculated at the level of BP86-D3/BS2, (BS2 = SDD for Ni and Fe and def2-TZVP for the other toms) with the SMD model. The integrals were evaluated by a pruned grid consisting of 99 radial shells and 590 angular points per shell. The wave function stability was checked for all metal complexes.

Initial approximations of the TSs were obtained by the AFIR methodology,[30] where the two-layer N-layered integrated molecular orbital and molecular mechanics (ONIOM) method was applied.[31] The ONIOM partitioning of the molecular system is shown in Fig. 2a. The BP86 functional was applied for the high level, using the SDD[26] basis set for Ni and Fe and the 3-21G basis sets[32] for the remaining atoms. The parametrization method 6 (PM6)[33] was applied for the low level. An artificial force parameter of 47.8 kcal/mol was used to explore the approximate reaction paths and TSs (Fig. 2b). The approximate TSs obtained by the AFIR method were finally optimized at the SMD/BP86-D3/BS1 level. The different use of basis set adapted in this study is that we used previous studies[14,11] to avoid high computational cost in the geometry optimization and obtain the energy accuracy.

Results and discussion

IR spectra of the three isomers of the NiFe hydride complex

The IR spectra of three isomers of the NiFe hydride complex were measured in our previous study.[11] However, the vibrational modes of some significant peaks are still unknown. Therefore, the peaks were assigned here.

Fig. 3 shows the calculated IR spectra of the NiFe hydride complexes (**2a, 2b, and 2c**), and Table 1 summarizes the theoretically calculated key stretch modes and the experimental parameters. Although scaling has been proposed for frequencies calculated by the DFT calculations to predict vibration peaks more precisely in experiments,[34] no such scaling was applied in this study. It is well-known that the stretching of the C=O bond is sensitive to the electron density of the metal owing to π-electron back donation. The calculated peaks of the stretching of the C=O bond of **2a** perfectly agree with the experimental value. Those of **2b** and **2c** were also reasonably consistent. The frequencies were in the following order: **2a** > **2b** > and **2c** from the high-frequency side, and this order also agrees with the experimental results.

The Ni–H stretching mode, which was not identified in the experimental study, of Complex **2a** appeared at 1037 cm^{-1}. Its peak appeared in the lower frequency region than that of the Fe–H stretching mode (1651 cm^{-1}), indicating that the interaction between Ni and the hydride was weaker than that between Fe and the hydride. The frequency of the Fe−H stretching mode (1651 cm^{-1}) of the bridging hydride (Complex **2a**) was close to that of the Fe–H stretching mode of another previously reported NiFe hydride complex (1687 cm^{-1}).[13] The peaks in the terminal hydrides, **2b,** and **2c**, were in a higher frequency region than the bridging hydride, **2a**.

The Fe–H stretching mode of **2b** was not identified in the experiment. The computational results revealed that the Fe–H stretching mode strongly coupled with the C=O stretching mode in **2b**. Particularly, the peaks at 1894 and 1829 cm^{-1} (Table 1) exhibited the contributions of the C=O and Fe–H stretching modes, respectively.

Isomerization of the hydride complexes

Next, the isomerization pathways of the hydride complexes were investigated; four probable reaction processes were explored: (1) proton exchanges between the NiFe hydride complexes, (2) hydrogen atom exchanges between the NiFe hydride complexes, (3) hydride exchanges between the NiFe hydride complexes, and (4) hydride-transfer reaction within the NiFe hydride complex. Regarding (1)–(3) involving two elementary reactions, only the first ones, (R1) and (R2), were investigated. The free energy of the reaction was calculated in an acetone solvent as in the experiment.

• Intercomplex proton transfer

$[NiFe–H]^+ + [NiFe–H]^+ \rightarrow [NiFe–H_2]^{2+} + [NiFe]^0$ (R1)

• Intercomplex H atom transfer

$[NiFe–H]^+ + [NiFe–H]^+ \rightarrow [NiFe–H_2]^+ + [NiFe]^+$ (R2)

• Intercomplex hydride transfer

$[NiFe–H]^+ + [NiFe–H]^+ \rightarrow [NiFe–H_2]^0 + [NiFe]^{2+}$ (R3)

• Intracomplex hydride transfer

$[NiFe–H]^+ \rightarrow [NiFe–H]^{+\prime}$ (R4)

Table 2 summarizes the calculated free energies of (R1)–(R3). To investigate the spin states of the ground states of the products in each reaction, we calculated four spin states; S = 0, 1, 2, and 3 for $[NiFe\text{-}H_2]^{2+}$, $[NiFe\text{-}H_2]^0$, $[NiFe]^0$, and $[NiFe]^{2+}$, and S = 1/2, 3/2, 5/2, and 7/2 for $[NiFe\text{-}H_2]^+$ and $[NiFe]^+$. As a result, $[NiFe]^0$ showed a triplet state and all other complexes showed the lowest spin state. In $[NiFe\text{-}H_2]^0$ and $[NiFe]^0$, the energies of the singlet and triplet spin states are less than 5 kcal/mol, and they are presumed to be spin crossover complexes. The lowest energy spin state was used to estimate the free energy of the reaction. Two configurations were determined for the 2H bound to Fe (Fig. S2), and the lower energy configuration was selected. Consequently, (R1)–(R3) were highly endergonic reactions, and we predicted that none of them would occur.

Thereafter, we examined the possibility of producing these isomers via hydride transfer within the NiFe hydride complex (R4). Our previous studies revealed that all the isomers exhibited singlet ground states. Thus, the energy of the lowest singlet state was calculated. The initial structure of the TS of intramolecular hydride transfer was generated manually rather than via AFIR.

Fig. 4 shows the calculated free energy profile for the isomerization of the NiFe hydride complex. The calculated thermodynamic stabilities of the three hydride complexes in acetone were in the following order: **2a** > **2c** > **2b**. The bridging hydride complex was more stable than the terminal hydrides of the binuclear complex.

Table 3 summarizes the calculated reaction barriers and those derived from the experimental rate constant (*k*) based on the classical TS theory. Notably, two pathways were determined for the isomerization of **2b** to **2a**. One was direct (**2b** → **2a**), and the other involved an indirect path (**2b** → **2c** → **2a**), which exhibited a lower reaction barrier. The calculated reaction barriers of all the isomerization reactions correlated well with the experimental data.

The bridging hydrides in the NiFe hydrogenase enzymes were the intermediates for H_2 activation.[35] The terminal hydrides in the FeFe hydrogenase enzymes were detected via nuclear resonance spectroscopy (NMR).[9,10] These hydrides were detected in the most thermodynamically stable and major intermediate. However, the detections of multiple hydride complex isomers in this NiFe hydrogenase model complex[11] and the previously studied FeFe hydrogenase model complex[36] indicated the possible existence of other hydride coordination states in each enzyme as short-lived states.

Electron, proton, and hydride transfers in the three hydride complex isomers

Next, we investigated the reactivities of the three isomers of the hydride complex toward electron, proton, and hydride transfers. The experimentally determined percentages of the electron transfer, H_2 production, and H transfer product yields at specific times are summarized in (Table S2). Experimentally demonstrated different reactivity of the three hydride isomers indicates that the isomerization reaction proceeds more slowly than the electron transfer, hydride transfer, and proton transfer reactions.

Electron-transfer reaction. The redox process is fundamental to biological enzymes. The Fe–S cluster in the NiFe hydrogenase enzyme acts as the mediator of the electron transport.[37,38,39] In this study's NiFe hydrogenase model system, ferrocene, which undergoes one-electron reduction, was employed as an oxidant. The reaction energy (R5) of the NiFe hydride complex containing ferrocene was calculated to investigate the susceptibility of the NiFe hydride complex to oxidation.

$\mathbf{X} + [Fe^{III}(C_5Me_5)_2]^+ \rightarrow {}^{2}\mathbf{X}^{2+} + [Fe^{II}(C_5Me_5)_2]$ (**X** = **2a**, **2b**, and **2c**) (R5)

The calculated free energies of the three isomers were negative (Table 4), thus corroborating the experimental data, which revealed that the NiFe hydride complexes were oxidized by ferrocene. Further, the free energies of Complexes **2a** and **2c** were more negative than that of **2b**, indicating that **2a** and **2c** were more susceptible to oxidation than **2b**.

A less computationally intensive method could be employed to compare or predict the electron-donating capacities of multiple complexes. We investigated whether the ionization energy could quantitatively predict the electron-donating capacities of the complexes. The ionization energy was calculated employing three approaches. The first approach applies the adiabatic IP (given as the energy difference between the non-oxidized NiFe complex and the one-electron oxidized complex). The energy of each state is calculated employing an optimized structure of each redox state. The second uses the vertical ionization energy (each state's energy is estimated for the optimized structure of the non-oxidized complex. The third employs IP, which is estimated according to the IP theorem.[40] In this theorem, IP is estimated as a minus of the HOMO energy. All IP calculations are performed employing SMD solvation model to consider the solvation effects.

The calculated adiabatic IP and IP theorem (Table 4) indicated that Complex **2a** (the bridging hydride) was the most susceptible to oxidization, followed by Complexes **2c** and **2b** (the terminal hydrides). This result is consistent with the experimental observation that Complex **2a** was more susceptible to oxidation than Complexes **2b** and **2c**. However, the vertical IP did not correctly predict the orders between **2b** and **2c**, indicating that geometric changes due to oxidation cannot be ignored. The calculated ionization potentials

should also correlate with the experimentally observed redox potentials. However, the experimentally measured redox potentials are -2.04, -2.04, and -2.06 V for **2a**, **2b**, and **2c**, respectively, indicating that the electron-donating ability is almost the same. Therefore, the calculated adiabatic ionization potentials more closely correlate to the experimentally observed product yields of the electron transfer reaction to ferrocene (Table S2).

The spin density of the one-electron oxidized hydride complex was evenly distributed in Ni and Fe for all three isomers (Table 4). This result is consistent with the HOMO distribution (Fig. 4), indicating that Ni and Fe could act as active sites for chemical reactions after the one-electron oxidation process.

Thermodynamic hydricity and kinetics of hydride transfer. Hydricity,[41] which is a valuable quantity that indicates the ease of hydride transfer, was investigated, particularly in relation to the reactivities of hydride complexes in CO_2 reduction[5,6,42,43] and H_2 production.[44,45] The hydride transfers in NiFe complexes (**2a–2c**) in the presence of methylene blue (MB) have been demonstrated.[11] However, it is unclear whether the reaction is controlled by thermodynamics or kinetics.

Fig. 6 shows the calculated free energy profile of the transfer of hydrides from the hydride complex into MB in an acetonitrile solution. For **2b** and **2c**, the hydride was extracted directly from Fe; however, in **2a**, it was bound first to the carbonyl group (**3a'**), after which it moved into MB. After the extraction of the hydride, the solvent (CH_3CN) coordinated Fe in **2b** and **2c**, whereas it retained empty sites in **2a** (Table S3).

Several schemes have been proposed to calculate the hydricity.[41,46] The relative hydricity is estimated as the free energy change in the hydride-transfer reaction (R5):

$$\text{NiFe–H} + \text{MB}^+ \rightarrow \text{NiFe} + \text{MBH}, \qquad \text{(R5)}$$

where MBH is reduced MB by a hydride; the atomic site that accepts the hydride is nitrogen. The relative hydricity exhibits an advantage: it can only be calculated from the calculated values without employing the experimental ones. In (R5), MB was consistently utilized as the hydride acceptor for the three isomers; thus, the difference in the reaction energy arose only from the electronic states of the isomers. However, it is well-known that the changes in the hydricity depend on the solvent.[46] Thus, in this study, the hydricity was evaluated considering the explicit solvent coordination to the Fe site after the removal of the hydride.

The calculated relative hydricities were in the following descending order: **2b** (13.8 kcal/mol) > **2a** (5.8 kcal/mol) > **2c** (5.6 kcal/mol). Moreover, the height of the barrier was in the following ascending order: **2b** < **2c** < **2a**. Thus, the terminal hydride kinetically and thermodynamically favored hydride transfer, which is consistent with the experimental observation. Conversely, the results of this calculation are inconsistent with the experimental observations, which indicated that **2c** was most susceptible to hydride transfer than **2b**.

Energy decomposition analysis (EDA) was applied to elucidate the origin of the barrier height. The activation energy, ΔE_{act}, of the hydride-transfer reaction can be divided into two terms, as follows:

$$\Delta E_{act} = \Delta E_{def} + \Delta E_{int}, \qquad (1)$$

where the terms ΔE_{def} and ΔE_{int} are the deformation and interaction energies, respectively. The deformation energy corresponds to the energy difference that originated from structural changes toward TS formation. The interaction energy is the energy difference between the catalyst plus the substrate and complex in the TS structure (Fig. 7).

Table 5 summarizes the calculated deformation and interaction energies that did not exhibit ZPEs. The deformation energy of **2b** was the smallest (15.2 kcal/mol) among those of the three isomers. This small deformation energy of **2b** compared with those of **2a** and **2c** was due to the deformation energy of NiFe–H, not MB. Further, **2b** exhibited a larger interaction energy than **2c**, and the difference from **2a** was < 5 kcal/mol; its activation energy was the smallest among the three isomers.

The kinetic isotope effect (KIE) is one useful method to verify the reaction mechanism.[47,48] The KIE of the hydride transfer was not determined experimentally but was calculated in anticipation of later experimental studies. Table S4 summarizes the reaction barriers, rate constants for the case where hydrogen (H) is replaced by deuterium (D), and KIEs. As a result, the reaction barrier enhanced 3~5 kcal/mol with the replacement of H to D, and the larger KIE value was obtained for hydride complexes **2b** and **2c** compared to **2a**.

H_2 evolution. The evolution of H_2 is the reverse reaction of hydrogen activation, and the mechanisms were revealed in our previous study.[12] The active site for H_2 evolution is Fe, rather than Ni, different from the NiFe hydrogenase. Fig. 8 shows a comparison between the free energy profiles of H_2 evolution for the three NiFe hydride complex isomers. Hydrogen production employing the NiFe complex proceeds via two steps: (1) the transfer of proton from the Brønsted acid (acetic acid) to the Fe-center of the NiFe hydride complex, and (2) the dissociation of H_2 from the Fe-center. In the final products, we investigated the possibility of binding between the solvent water molecules and the empty sites that were generated via the dissociation of H_2. Thus, the coordination of H_2O destabilizes the complex in all the isomers (Table S3). Therefore, the possibility of H_2O binding was excluded.

The free energy profile indicated that Complex **2b** was best suited to generating hydrogen because it is kinetically advantageous, and the reaction was the most exergonic. This result correlates with the experimental observations (Table S2). The lowered energy of TS during H_2 dissociation in Complex **2b** was due to the thermodynamic corrections (Table S6). Regarding Complex **2a**, the reaction was almost thermoneutral, indicating that the bridging hydride complex facilitated H_2 activation and production. Conversely, in the other terminal hydride complex (**2c**), the calculated reaction was ~10 kcal/mol endergonic; **2c** was more suitable for H_2 activation than H_2 production. The experimental study revealed that hydrogen production occurred in Complex **2c** (Table S2), although the yield of the product was low. This is probably because of the low concentration of the produced H_2, and the unlikeliness of the reverse reaction to occur. Our previous study revealed that a highly acidic medium favored the transfer of protons into the NiFe hydride complex. Further, the acidity affected both the reaction barrier and energy. These results demonstrated that finetuning the basicity/acidity would probably alter the reaction in **2a**, which exhibited almost total thermoneutrality for H_2 activation and evolution.

Removing hydrogen from the dihydride during the second step was easiest in **2b** than in the other complexes. This H_2-removal capacity

could be attributed to the Fe–H distance in the dihydrogen complex. The longest and shortest Fe–H distances were observed in **2b** (1.70 and 1.71 Å, Fig. 5) and **2c** (1.58 and 1.58 Å, Fig. 5), respectively.

Conclusions

In this study, we elucidated the mechanism of the isomerization of the NiFe hydride complex. Further, we quantitatively discussed the electron- and hydride-donating abilities of the three isomers of the hydride complex, as well as their efficiencies for H_2 evolution. The findings in this study are as follows:

(1) The bridging hydride complex exhibited lower energy than the terminal hydride complex, and the three isomers were interconverted via hydride transfers within the complex.

(2) The calculated adiabatic IP of the NiFe hydride complex indicated that the bridging hydrides were more susceptible to electron oxidation than the terminal hydrides. The same trend was predicted from the HOMO energy.

(3) The terminal hydrides were more susceptible to hydride transfer than the bridging hydrides. In the terminal hydride, the hydride was extracted directly into MB, but it moved into MB via the intermediate in which the hydride was bound to the CO ligand in the bridging hydride. EDA revealed that the hydride transfer's reaction barrier was dominantly controlled by the structural deformation of the NiFe hydride complex.

(4) The terminal hydrides exhibited thermodynamic and kinetic advantages over the bridging hydrides for hydrogen production.

Conflicts of interest

There are no conflicts of interest to declare.

Acknowledgements

This work was in part supported by World Premier International Research Center Initiative (WPI), Grants-in-Aid for Scientific Research (KAKENHI JP18K05297 and JP26000008), JST CREST Grant Number JPMJCR18R2. Computer resources at the Academic Center for Computing and Media Studies at Kyoto University, Research Center of Computer Science at the Institute for Molecular Science are also acknowledged.

References

1 A. J. Esswein and D. G. Nocera, Hydrogen Production by Molecular Photocatalysis, *Chem. Rev.* 2007, **107**, 4022-4047.

2 J. Zhang, X. Bai, T. Wang, W. Xiao, P. Xi, J. Wang, D. Gao and J. Wang, Bimetallic Nickel Cobalt Sulfide as Efficient Electrocatalyst for Zn-Air Battery and Water Splitting, *Nanomicro Lett* 2019, **11**, 2.

3 E. Kounalis, M. Lutz and D. L. J. Broere, Cooperative H_2 Activation on Dicopper(I) Facilitated by Reversible Dearomatization of an "Expanded PNNP Pincer" Ligand, *Chemistry* 2019, **25**, 13280-13284.

4 R. C. Cammarota, L. J. Clouston and C. C. Lu, Leveraging Molecular Metal–Support Interactions for H_2 and N_2 Activation, *Coord. Chem. Rev.* 2017, **334**, 100-111.

5 D. L. Dubois and D. E. Berning, Hydricity of Transition-Metal Hydrides and Its Role in CO_2 Reduction, *Appl. Organomet. Chem.* 2000, **14**, 860-862.

6 K. M. Waldie, A. L. Ostericher, M. H. Reineke, A. F. Sasayama and C. P. Kubiak, Hydricity of Transition-Metal Hydrides: Thermodynamic Considerations for CO_2 Reduction, *ACS Catal.* 2018, **8**, 1313-1324.

7 K. S. Sandhya and C. H. Suresh, Designing Metal Hydride Complexes for Water Splitting Reactions: A Molecular Electrostatic Potential Approach, *Dalton Trans* 2014, **43**, 12279-12287.

8 H. Ogata, T. Kramär, H. Wang, D. Schilter, V. Pelmenschikov, M. Van Gastel, F. Neese, T. B. Rauchfuss, L. B. Gee, A. D. Scott, Y. Yoda, Y. Tanaka, W. Lubitz and S. P. Cramer, Hydride Bridge in [NiFe]-Hydrogenase Observed by Nuclear Resonance Vibrational Spectroscopy, *Nat. Commun.* 2015, **6**, 7890.

9 E. J. Reijerse, C. C. Pham, V. Pelmenschikov, R. Gilbert-Wilson, A. Adamska-Venkatesh, J. F. Siebel, L. B. Gee, Y. Yoda, K. Tamasaku, W. Lubitz, T. B. Rauchfuss and S. P. Cramer, Direct Observation of an Iron-Bound Terminal Hydride in [FeFe]-Hydrogenase by Nuclear Resonance Vibrational Spectroscopy, *J. Am. Chem. Soc.* 2017, **139**, 4306-4309.

10 S. Rumpel, C. Sommer, E. Reijerse, C. Farès and W. Lubitz, Direct Detection of the Terminal Hydride Intermediate in [FeFe] Hydrogenase by NMR Spectroscopy, *J. Am. Chem. Soc.* 2018, **140**, 3863-3866.

11 S. Ogo, T. Kishima, T. Yatabe, K. Miyazawa, R. Yamasaki, T. Matsumoto, T. Ando, M. Kikkawa, M. Isegawa, K. S. Yoon and S. Hayami, [NiFe], [FeFe], and [Fe] hydrogenase models from isomers, *Sci. Adv.* 2020, **6**, eaaz8181.

12 M. Isegawa, T. Matsumoto and S. Ogo, H_2 activation by hydrogenase-inspired NiFe catalyst using frustrated Lewis pair: effect of buffer and halide ion in the heterolytic H–H bond cleavage, *RSC Adv.* 2021, **11**, 28420-28432.

13 S. Ogo, K. Ichikawa, T. Kishima, T. Matsumoto, H. Nakai, K. Kusaka and T. Ohhara, A functional [NiFe]hydrogenase mimic that catalyzes electron and hydride transfer from H_2, *Science (New York, N.Y.)* 2013, **339**, 682-684.

14 M. Isegawa, A. K. Sharma, S. Ogo and K. Morokuma, Electron and Hydride Transfer in a Redox-Active NiFe Hydride Complex: A DFT Study, *ACS Catal.* 2018, **8**, 10419-10429.

15 M. Z. Makos, M. Freindorf, D. Sethio and E. Kraka, New insights into Fe-H-2 and Fe-H- bonding of a [NiFe] hydrogenase mimic: a local vibrational mode study, *Theor. Chem. Acc.* 2019, **138**.

16 D. Brazzolotto, L. K. Wang, H. Tang, M. Gennari, N. Queyriaux, C. Philouze, S. Demeshko, F. Meyer, M. Orio, V. Artero, M. B. Hall and C. Duboc, Tuning Reactivity of Bioinspired [NiFe]-Hydrogenase Models by Ligand Design and Modeling the CO Inhibition Process, *ACS Catal.* 2018, **8**, 10658-10667.

17 M. J. T. Frisch, G. W.; Schlegel, H. B.; Scuseria, G. E.; Robb, M. A.; Cheeseman, J. R.; Scalmani, G.; Barone, V.; Mennucci, B.; Petersson, G. A.; Nakatsuji, H.; Caricato, M.; Li, X.; Hratchian, H. P.; Izmaylov, A. F.; Bloino, J.; Zheng, G.; Sonnenberg, J. L.; Hada, M.; Ehara, M.; Toyota, K.; Fukuda, R.; Hasegawa, J.; Ishida, M.; Nakajima, T.; Honda, Y.; Kitao, O.; Nakai, H.; Vreven, T.; Montgomery, J. A., Jr.; Peralta, J. E.; Ogliaro, F.; Bearpark, M.; Heyd, J. J.; Brothers, E.; Kudin, K. N.; Staroverov, V. N.; Kobayashi, R.; Normand, J.; Raghavachari, K.; Rendell, A.; Burant, J. C.; Iyengar, S. S.; Tomasi, J.; Cossi, M.; Rega, N.; Millam, J. M.; Klene, M.; Knox, J. E.; Cross, J. B.; Bakken, V.; Adamo, C.; Jaramillo, J.; Gomperts, R.; Stratmann, R. E.; Yazyev, O.; Austin, A. J.; Cammi, R.; Pomelli, C.; Ochterski, J. W.; Martin, R. L.; Morokuma, K.; Zakrzewski, V. G.; Voth, G. A.; Salvador, P.; Dannenberg, J. J.; Dapprich, S.; Daniels, A. D.; Farkas, Ö.; Foresman, J. B.; Ortiz, J. V.;

Cioslowski, J.; Fox, D. J., *Gaussian 09, Revision E.01; Gaussian, Inc.: Wallingford, CT* 2009.

18 A. D. Becke, Density Functional Calculations of Molecular Bond Energies, *J. Chem. Phys.* 1986, **84**, 4524-4529.

19 J. P. Perdew, Density-Functional Approximation for the Correlation-Energy of the Inhomogeneous Electron-Gas, *Phys. Rev. B* 1986, **33**, 8822-8824.

20 S. Grimme, J. Antony, S. Ehrlich and H. Krieg, A Consistent and Accurate Ab Initio Parametrization of Density Functional Dispersion Correction (DFT-D) for the 94 Elements H-Pu, *J. Chem. Phys.* 2010, **132**, 154104.

21 M. Bruschi, M. Tiberti, A. Guerra and L. De Gioia, Disclosure of Key Stereoelectronic Factors for Efficient H_2 Binding and Cleavage in the Active Site of [NiFe]-Hydrogenases, *J. Am. Chem. Soc.* 2014, **136**, 1803-1814.

22 M. Kampa, M. E. Pandelia, W. Lubitz, M. Van Gastel and F. Neese, A metal-metal bond in the light-induced state of [NiFe] hydrogenases with relevance to hydrogen evolution, *J. Am. Chem. Soc.* 2013, **135**, 3915-3925.

23 O. A. Ulloa, M. T. Huynh, C. P. Richers, J. A. Bertke, M. J. Nilges, S. Hammes-Schiffer and T. B. Rauchfuss, Mechanism of H_2 Production by Models for the [NiFe]-Hydrogenases: Role of Reduced Hydrides, *J. Am. Chem. Soc.* 2016, **138**, 9234-9245.

24 H. Tang and M. B. Hall, Biomimetics of [NiFe]-Hydrogenase: Nickel- or Iron-Centered Proton Reduction Catalysis?, *J. Am. Chem. Soc.* 2017, **139**, 18065-18070.

25 M. Isegawa, T. Matsumoto and S. Ogo, Selective Oxidation of H_2 and CO by Nilr Catalyst in Aqueous Solution: A DFT Mechanistic Study, *Inorg. Chem.* 2020, **59**, 1014-1028.

26 M. Dolg, U. Wedig, H. Stoll and H. Preuss, Ab initio Pseudopotential Study of the 1st Row Transition-Metal Monoxides and Iron Monohydride, *J. Chem. Phys.* 1987, **86**, 2123-2131.

27 F. Weigend and R. Ahlrichs, Balanced Basis Sets of Split Valence, Triple Zeta Valence and Quadruple Zeta Valence Quality for H to Rn: Design and Assessment of Accuracy, *Phys. Chem. Chem. Phys.* 2005, **7**, 3297-3305.

28 A. V. Marenich, C. J. Cramer and D. G. Truhlar, Universal Solvation Model Based on the Generalized Born Approximation with Asymmetric Descreening, *J. Chem. Theory Comput.* 2009, **5**, 2447-2464.

29 K. Fukui, The Path of Chemical-Reactions - the IRC Approach, *Acc. Chem. Res.* 1981, **14**, 363-368.

30 S. Maeda and K. Morokuma, Finding Reaction Pathways of Type A+B -> X: Toward Systematic Prediction of Reaction Mechanisms, *J. Chem. Theory Comput.* 2011, **7**, 2335-2345.

31 F. Maseras and K. Morokuma, IMOMM - a New Integrated Ab-Initio Plus Molecular Mechanics Geometry Optimization Scheme of Equilibrium Structures and Transition-States, *J. Comput. Chem.* 1995, **16**, 1170-1179.

32 J. S. Binkley, J. A. Pople and W. J. Hehre, Self-Consistent Molecular-Orbital Methods .21. Small Split-Valence Basis-Sets for 1st-Row Elements, *J. Am. Chem. Soc.* 1980, **102**, 939-947.

33 J. J. P. Stewart, Optimization of Parameters for Semiempirical Methods V: Modification of NDDO Approximations and Application to 70 Elements, *J. Mol. Model.* 2007, **13**, 1173-1213.

34 M. K. Kesharwani, B. Brauer and J. M. Martin, Frequency and zero-point vibrational energy scale factors for double-hybrid density functionals (and other selected methods): can anharmonic force fields be avoided?, *J. Phys. Chem. A* 2015, **119**, 1701-1714.

35 H. Ogata, K. Nishikawa and W. Lubitz, Hydrogens Detected by Subatomic Resolution Protein Crystallography in a [NiFe] Hydrogenase., *Nature* 2015, **520**, 571-574.

36 B. E. Barton, G. Zampella, A. K. Justice, L. De Gioia, T. B. Rauchfuss and S. R. Wilson, Isomerization of the hydride complexes $[HFe_2(SR)_2(PR_3)(x)(CO)_{6-x}]^+$ (x=2, 3, 4) relevant to the active site models for the [FeFe]-hydrogenases, *Dalton. Trans.* 2010, **39**, 3011-3019.

37 M. E. Pandelia, H. Ogata and W. Lubitz, Intermediates in the Catalytic Cycle of [NiFe] Hydrogenase: Functional Spectroscopy of the Active Site, *Chemphyschem* 2010, **11**, 1127-1140.

38 T. Kramer, M. Kamp, W. Lubitz, M. Van Gastel and F. Neese, Theoretical Spectroscopy of the Ni-II Intermediate States in the Catalytic Cycle and the Activation of [NiFe] Hydrogenases, *Chembiochem* 2013, **14**, 1898-1905.

39 H. S. Shafaat, O. Rudiger, H. Ogata and W. Lubitz, [NiFe] hydrogenases: A common active site for hydrogen metabolism under diverse conditions, *Biochim. Biophys. Acta Bioenergetics* 2013, **1827**, 986-1002.

40 C. G. Zhan, J. A. Nichols and D. A. Dixon, Ionization potential, electron affinity, electronegativity, hardness, and electron excitation energy: Molecular properties from density functional theory orbital energies, *J. Phys. Chem. A* 2003, **107**, 4184-4195.

41 E. S. Wiedner, M. B. Chambers, C. L. Pitman, R. M. Bullock, A. J. Miller and A. M. Appel, Thermodynamic Hydricity of Transition Metal Hydrides, *Chem Rev* 2016, **116**, 8655-8692.

42 B. Mondal, F. Neese and S. F. Ye, Toward Rational Design of 3d Transition Metal Catalysts for CO_2 Hydrogenation Based on Insights into Hydricity-Controlled Rate-Determining Steps, *Inorg. Chem.* 2016, **55**, 5438-5444.

43 H. Fong and J. C. Peters, Hydricity of an Fe-H Species and Catalytic CO_2 Hydrogenation, *Inorg. Chem.* 2015, **54**, 5124-5135.

44 R. M. Bullock, A. M. Appel and M. L. Helm, Production of hydrogen by electrocatalysis: making the H-H bond by combining protons and hydrides, *Chem. Commun.* 2014, **50**, 3125-3143.

45 A. L. Ostericher, K. M. Waldie and C. P. Kubiak, Utilization of Thermodynamic Scaling Relationships in Hydricity To Develop Nickel Hydrogen Evolution Reaction Electrocatalysts with Weak Acids and Low Overpotentials, *ACS Catal.* 2018, **8**, 9596-9603.

46 K. R. Brereton, N. E. Smith, N. Hazari and A. J. M. Miller, Thermodynamic and kinetic hydricity of transition metal hydrides, *Chem. Soc. Rev.* 2020, **49**, 7929-7948.

47 M. Gomez-Gallego and M. A. Sierra, Kinetic isotope effects in the study of organometallic reaction mechanisms, *Chem Rev* 2011, **111**, 4857-4963.

48 D. Mandal, D. Mallick and S. Shaik, Kinetic Isotope Effect Determination Probes the Spin of the Transition State, Its Stereochemistry, and Its Ligand Sphere in Hydrogen Abstraction Reactions of Oxoiron(IV) Complexes, *Acc. Chem. Res.* 2018, **51**, 107-117.

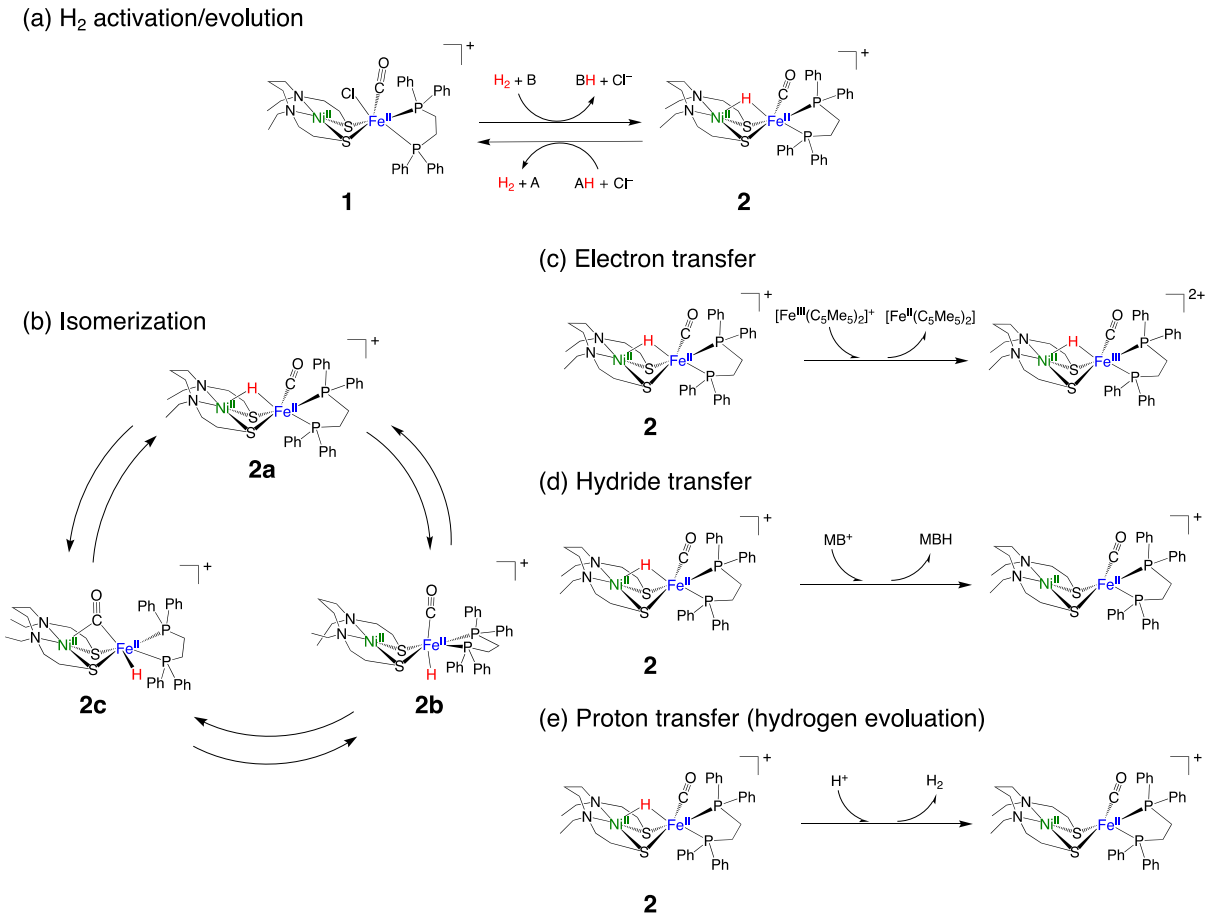

Fig. 1. (a) H_2 activation/evolution by the NiFe complex, (b) isomerization of the NiFe hydride complex, (c) electron transfer to ferrocene, $[Fe^{III}(C_5Me_5)_2]^+$, (d) hydride transfer to MB , and (e) proton transfer from acetic acid to the NiFe hydride complex during H_2 evolution

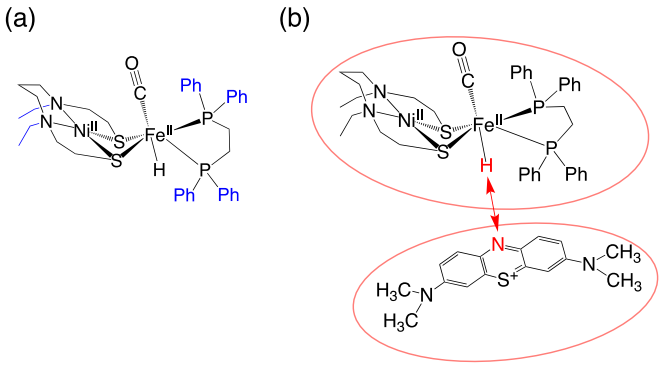

Fig. 2 (a) ONIOM partitioning. The black and blue parts are treated at high and low levels, respectively. (b) Fragmentation in the AFIR study. The artificial force was applied between the two red atoms.

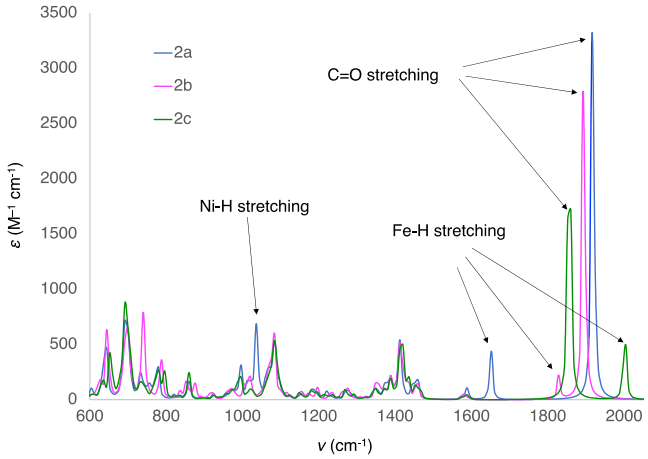

Fig. 3 Calculated infrared spectra of the three isomers of the NiFe hydride complexes (**2a**, **2b**, and **2c**)

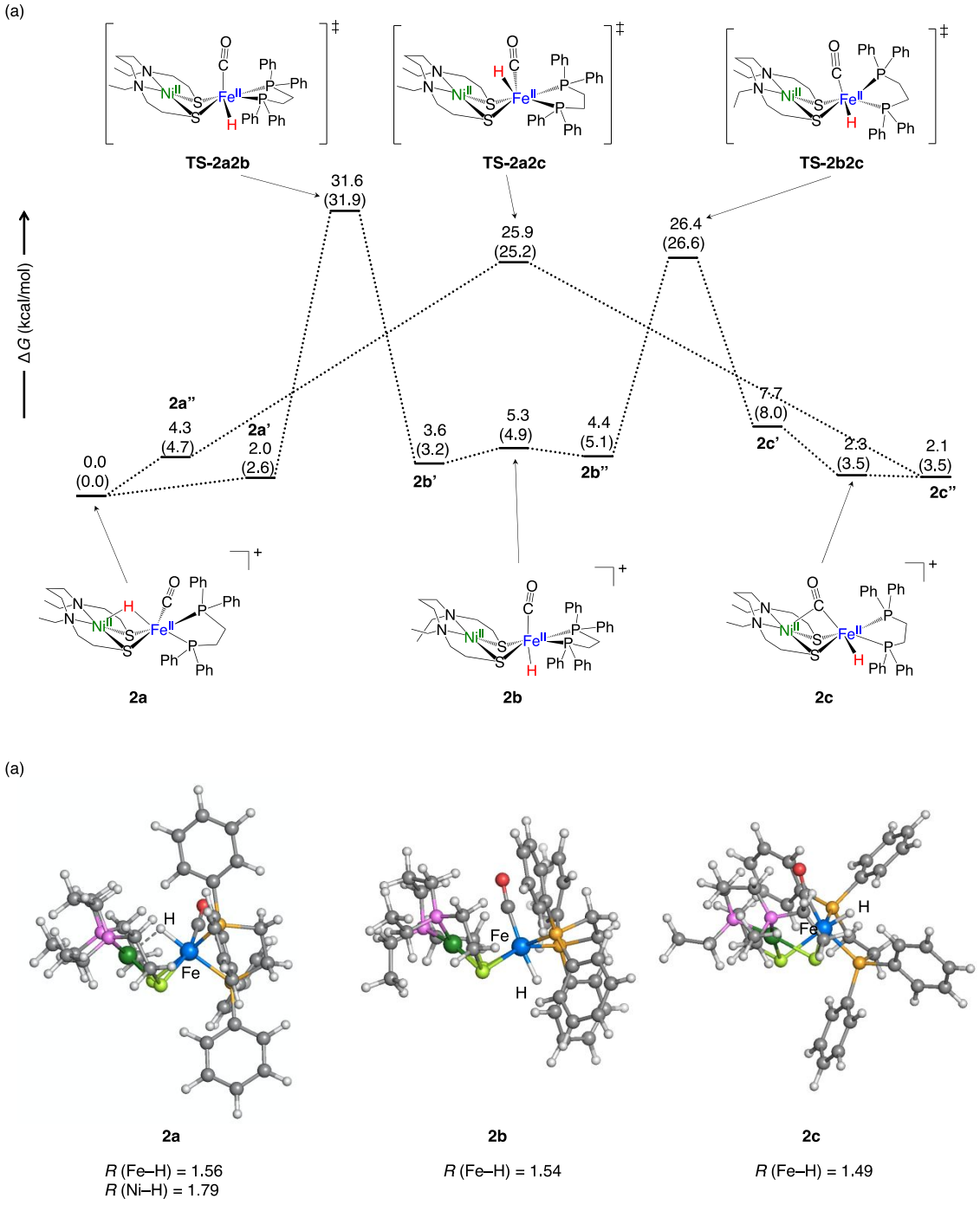

Fig. 4 (a) Calculated free energy profile for the isomerization of the NiFe hydride complex in acetone. Δ*G* and Δ*H* values (in parentheses) are reported in kcal/mol. (b) Optimized geometries of the hydride complexes (**2a**, **2b**, and **2c**) with the selected bond distances (Å)

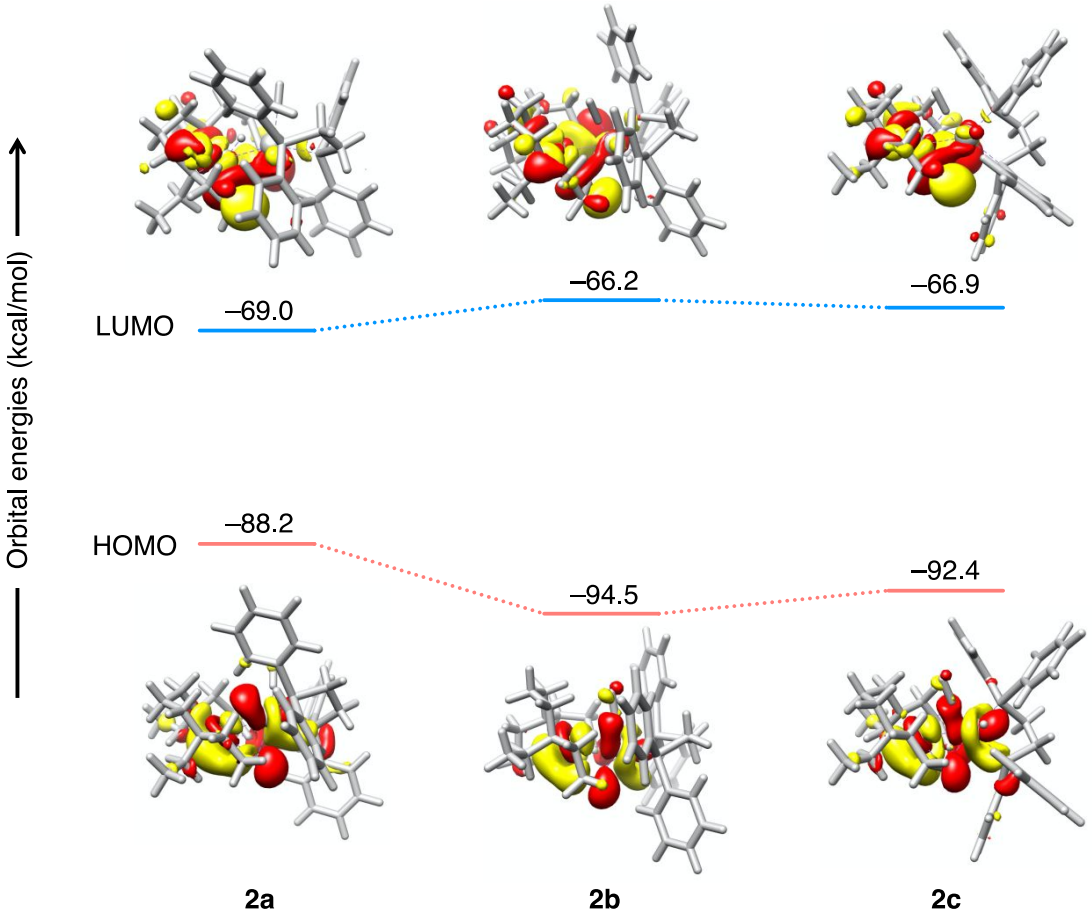

Fig. 5 HOMO and LUMO energies (kcal/mol) of the three isomers of the NiFe hydride complex (**2a**, **2b**, and **2c)**

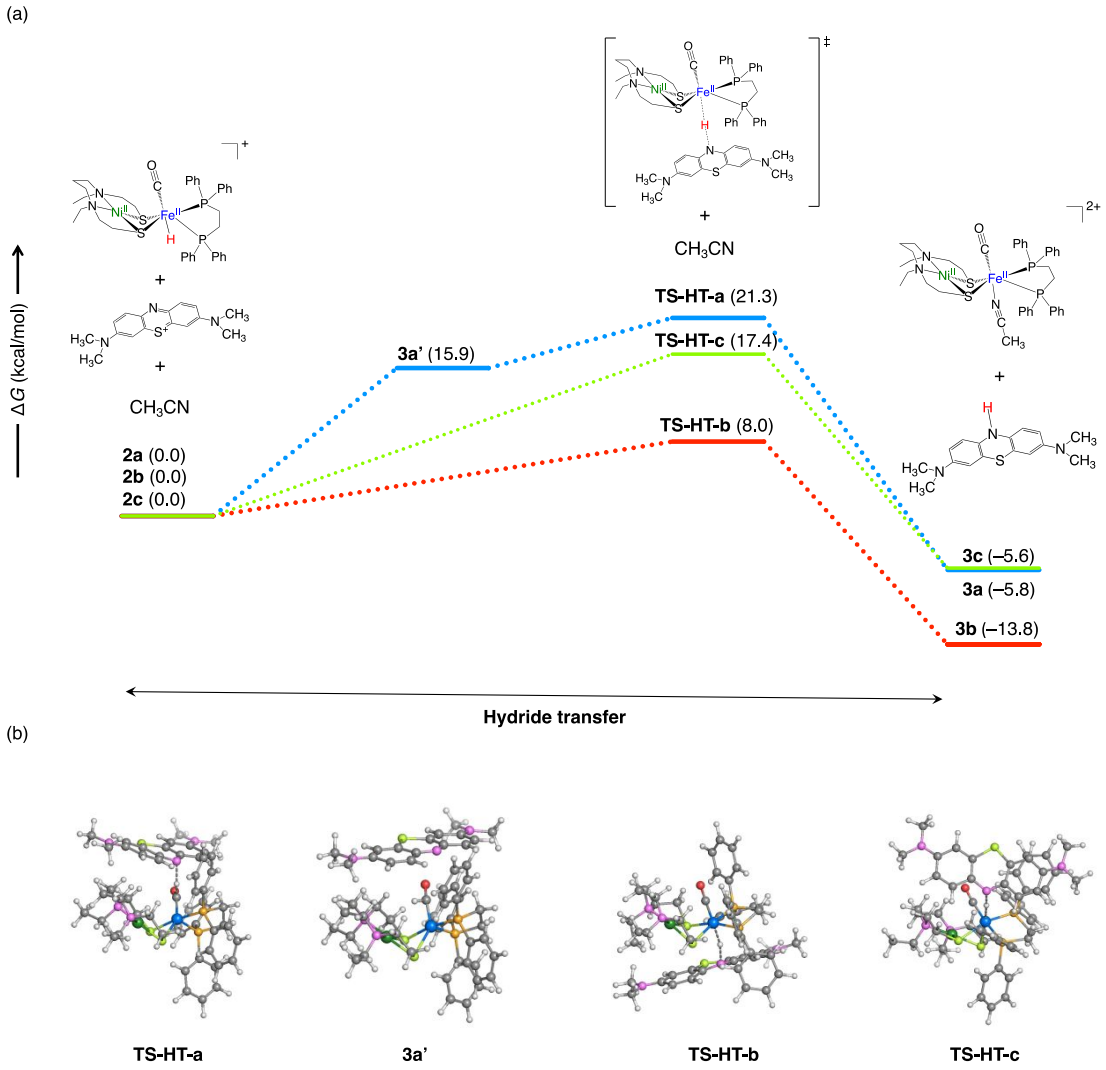

Fig. 6 (a) Calculated free energy profile for the transfer of the hydride from the NiFe hydride complex into MB (kcal/mol) in an acetonitrile solution. Δ*G* values (in parentheses) are reported in kcal/mol. (b) Optimized geometries of the TSs and intermediates

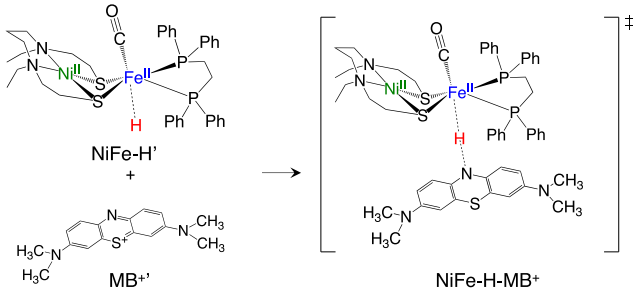

$$\text{NiFe-H} + \text{MB}^+ \xrightarrow{\Delta E_{def}} \text{NiFe-H'} + \text{MB}^{+\prime} \xrightarrow{\Delta E_{int}} \text{NiFe-H-MB}^+$$

$$\Delta E_{def} = \Delta E_{def}\,(\text{NiFe-H}) + \Delta E_{def}\,(\text{MB}^+)$$

Fig. 7. Schematic of EDA. NiFe-H' and MB$^{+\prime}$ represent the NiFe hydride complex and MB$^+$ at the TS structure. NiFe-H and MB$^+$ are the fully optimized structures of NiFe-H' and MB$^{+\prime}$, respectively.

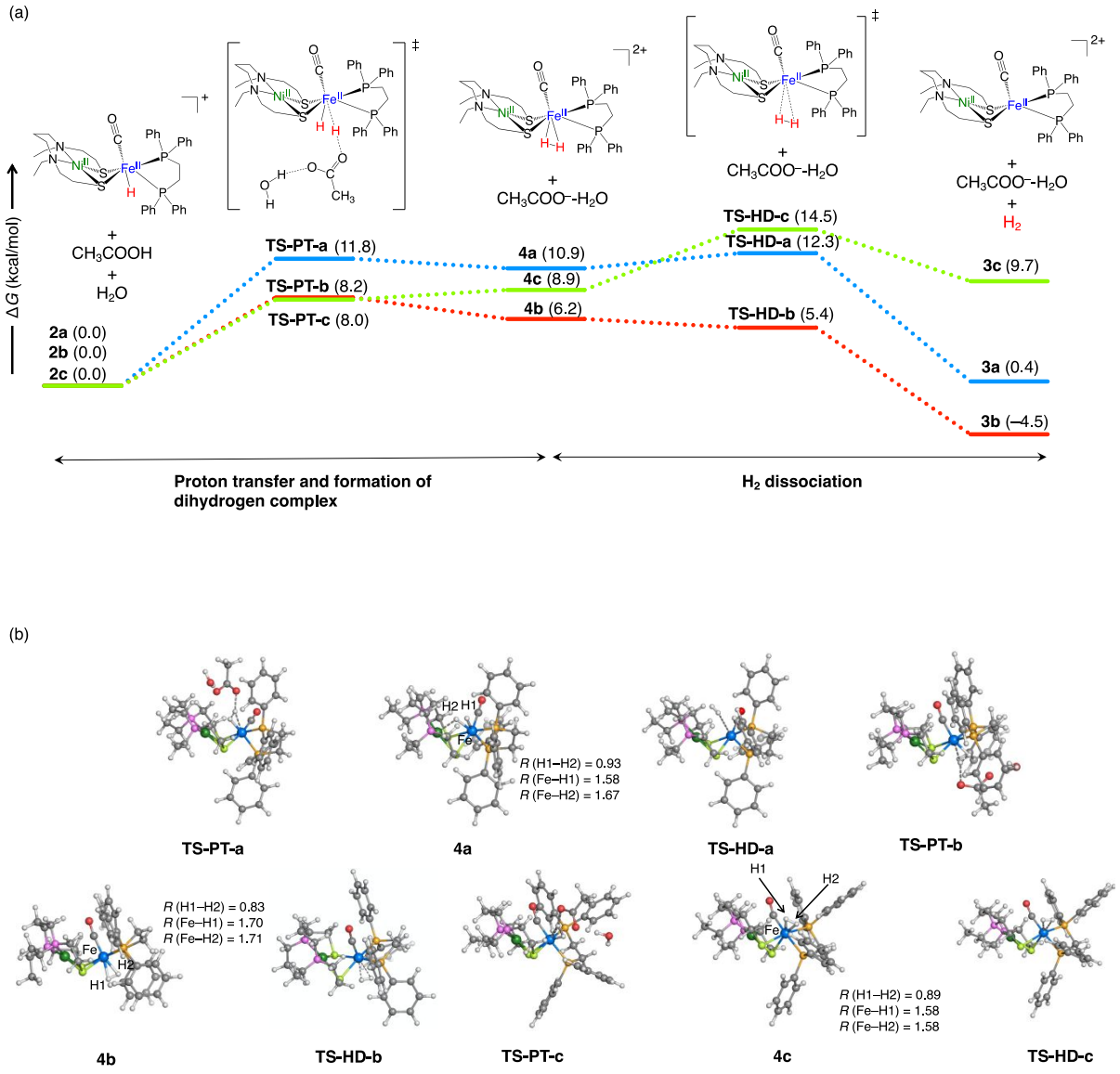

Fig. 8 (a) Calculated free energy profile for the evolution of H_2 from the hydride complex (kcal/mol) in an aqueous solution. Δ*G* values (in parentheses) are reported in kcal/mol. (b) Optimized geometries of the TSs and intermediates with the selected distances

Table 1 Calculated IR parameters (cm^{-1}) of the key stretching modes. Experimental parameters are in parenthesis

Complex	$\nu_{C=O}$	ν_{Ni-H}	ν_{Fe-H}
2a	1918 (1918)	1037[a]	1651 (1675)
2b	1894 (1910)	–	1829[a]
2c	1856 (1885)	–	2001 (1964)

[a] No experimental data

Table 2 Calculated free energies ΔG(kcal/mol) of (R1)–(R3)

		Δ*G*
(R1)	$[NiFe\text{-}H]^+ + [NiFe\text{-}H]^+ \rightarrow [NiFe\text{-}H_2]^{2+}$ (*S* = 0) + $[NiFe]^0$ (S = 1)	38.8
(R2)	$[NiFe\text{-}H]^+ + [NiFe\text{-}H]^+ \rightarrow [NiFe\text{-}H_2]^+$ (*S* = 1/2) + $[NiFe]^+$ (S = 1/2)	23.4
(R3)	$[NiFe\text{-}H]^+ + [NiFe\text{-}H]^+ \rightarrow [NiFe\text{-}H_2]^0$ (*S* = 0) + $[NiFe]^{2+}$ (S = 0)	32.0

Table 3 Calculated barrier heights of the hydride-transfer reaction (R4), as well as the experimental data

	2c → 2a	**2b→2a**	**2b→2c**
barrier (calc.)[a]	23.8	23.8[d]	22.7
barrier (exp.)[a,b]	23.3	24.0	22.9
k (exp.)[c]	1.1×10^{-4}	5.0×10^{-5}	1.5×10^{-5}

[a] In kcal/mol
[b] Estimated from the experimentally determined rate constant (*k*)
[c] In s^{-1}
[d] The barrier of the isomerization (**2c → 2a**)

Table 4 Free energies[a] of the electron-transfer reaction (R5) between the NiFe hydride complex and ferrocene, the ionization energies[a] of the NiFe hydride complex, and the spin densities of Ni and Fe of the one-electron oxidized hydride complex

	2a	**2b**	**2c**
		Reaction with ferrocene (R5)	
Δ*G*	−10.9	−6.9	−10.3
		IP	
IP (adiabatic)	96.5	100.5	97.1
IP (vertical)	97.6	99.0	101.2
IP (IP theorem)	88.2	94.5	92.4
		Spin density	
ρ (Ni)	0.50	0.38	0.41
ρ (Fe)	0.44	0.59	0.61

[a] Energies are in kcal/mol.

Table 5 EDA of the TS of hydride transfer in the three isomers

	ΔE_{def} (NiFe-H-MB)	ΔE_{def} (NiFe-H)	ΔE_{def} (MB)	ΔE_{int}	ΔE_{act}	ΔG_{act}
TS-HT-a	31.1	27.7	3.4	-25.8	5.2	21.3
TS-HT-b	15.2	10.9	4.3	-22.6	-7.4	8.0
TS-HT-c	22.8	18.6	4.1	-18.7	4.0	17.4